V. Conclusion

The achievable spectral efficiency for MIMO on-body channels has been evaluated, quantified, and investigated for discrete- and continuous-rate adaptive schemes in the on-body channels using MIMO PIFA antenna arrays at the transmitter and receiver sides. It has been shown that, due to the spatial subchannel correlation, the MIMO channel may be, at some instances, reduced to one equivalent eigenchannel, particularly in the case of the belt–chest channel. The increase in SNR value allows activating the second eigenmode in the belt–head channel, which exhibits low subchannel correlation, whereas the presence of a strong LOS component in the belt–chest channel may inhibit it whatever the SNR value. At the low-SNR range, using the discrete scheme allows achieving the same spectral efficiency as the continuous counterpart. Due to its aforementioned lower subchannel correlation, the belt–head channel is shown to offer better performance in terms of spectral efficiency, compared with the belt–chest channel, and slightly lower than the equivalent Rayleigh channel.

Acknowledgment

The authors would like to thank Dr. I. Khan for his valuable assistance and the two institutions CDTA in Algeria and FQRNT in Canada for their funding.

References

[1] P. S. Hall and Y. Hao, *Antennas and Propagation for Body-Centric Wireless Communications*. London, U.K.: Artech House, 2006.
[2] P. S. Hall, H. Yang, Y. I. Nechayev, A. Alomainy, C. C. Constantinou, C. Parini, M. R. Kamarudin, T. Z. Salim, D. T. M. Hee, R. Dubrovka, A. S. Owadally, S. Wei, A. Serra, P. Nepa, M. Gallo, and M. Bozzetti, "Antennas and propagation for on-body communication systems," *IEEE Antennas Propag. Mag.*, vol. 49, no. 3, Jun. 2007.
[3] A. Alomainy, Y. Hao, A. Owadally, C. Parini, Y. Nechayev, P. Hall, and C. C. Constantinou, "Statistical analysis and performance evaluation for on-body radio propagation with microstrip patch antennas," *IEEE Trans. Antennas Propag.*, vol. 55, no. 1, pp. 245–248, Jan. 2007.
[4] A. Fort, C. Desset, P. Wamacq, and L. V. Biesen, "Indoor body-area channel model for narrowband communications," *IET Microw., Antennas, Propag.*, vol. 1, no. 6, pp. 1197–1203, Dec. 2007.
[5] I. Khan, Y. Nechayev, K. Ghanem, and P. Hall, "BAN-BAN interference rejection with multiple antennas at the receiver," *IEEE Trans. Antennas Propag.*, vol. 58, no. 3, pp. 927–934, Mar. 2010.
[6] K. Ghanem, I. Khan, P. Hall, and L. Hanzo, "MIMO channel modeling and capacity of body area networks," *IEEE Trans. Antennas Propag.*, vol. 60, no. 6, pp. 2980–2986, Jun. 2012.
[7] I. Khan and P. S. Hall, "Experimental evaluation of MIMO capacity and correlation for narrowband body-centric wireless channels," *IEEE Trans. Antennas Propag.*, vol. 58, no. 1, pp. 195–202, Jan. 2010.
[8] Y. I. Nechayev and P. S. Hall, "Multipath fading of on-body propagation channels," in *Proc. IEEE Int. AP-S Symp.—USNC/URSI Nat. Radio Sci. Meeting*, San Diego, Jul. 2008, pp. 1–4.
[9] W. T. Webb and R. Steele, "Variable rate QAM for mobile radio," *IEEE Trans. Commun.*, vol. 43, no. 7, pp. 2223–2230, Jul. 1995.
[10] A. Goldsmith and P. Varaiya, "Variable-rate variable-power M-QAM for fading channels," in *Proc. IEEE. ICC*, May 1993, pp. 600–604.
[11] M.-S. Alouini and A. Goldsmith, "Capacity of Rayleigh fading channels under different adaptive transmission and diversity-combining techniques," *IEEE Trans. Veh. Technol.*, vol. 48, no. 4, pp. 1165–1181, Jul. 1999.
[12] *EE359—Wireless Communications*, Stanford Univ., 2011.
[13] K. Ghanem and T. A. Denidni, "Modified-rate-quantization algorithm for multiple-input multiple-output systems," *J. Wireless Pers. Commun.*, vol. 43, no. 4, pp. 1241–1255, Dec. 2007.
[14] G. J. Foschini and M. J. Gans, "On limits of Wireless communications in Fading Environment when using Multiple antennas," *Wireless pers. commun.*, vol. 6, no. 3, pp. 311–335, Mar. 1998.
[15] I. E. Telatar, "Capacity of multiantenna Gaussian channels," *Eur. Trans. Telecommun.*, vol. 10, no. 6, pp. 585–595, Nov./Dec. 1999.
[16] D. Shiu, G. J. Foschini, M. J. Gans, and J. M. Kahn, "Fading correlation and its effect on the capacity of multi-element antenna systems," *IEEE Trans. Commun.*, vol. 48, no. 3, pp. 502–513, Mar. 2000.
[17] R. E. Jaramillo, O. Fernandez, and R. P. Torres, "Empirical analysis of 2×2 MIMO channel in outdoor-indoor scenarios for BFWA applications," *IEEE Antennas Propag. Mag.*, vol. 48, no. 6, pp. 57–69, Dec. 2006.
[18] J. P. Kermoal, L. Schumacher, K. I. Pedersen, P. E. Mogensen, and F. Frederiksen, "A stochastic MIMO radio channel model with experimental validation," *IEEE J. Sel. Areas Commun.*, vol. 20, no. 6, pp. 1211–1226, Aug. 2002.

OFDMA/SC-FDMA Aided Space–Time Shift Keying for Dispersive Multiuser Scenarios

Mohammad Ismat Kadir, Shinya Sugiura, *Senior Member, IEEE*, Jiayi Zhang, Sheng Chen, *Fellow, IEEE*, and Lajos Hanzo, *Fellow, IEEE*

***Abstract*—Motivated by the recent concept of space–time shift keying (STSK), which was developed for achieving a flexible diversity versus multiplexing gain tradeoff, we propose a novel orthogonal frequency-division multiple access (OFDMA)/single-carrier frequency-division multiple-access (SC-FDMA)-aided multiuser STSK scheme for frequency-selective channels. The proposed OFDMA/SC-FDMA STSK scheme can provide an improved performance in dispersive channels while supporting multiple users in a multiple-antenna-aided wireless system. Furthermore, the scheme has the inherent potential of benefitting from the low-complexity single-stream maximum-likelihood detector. Both an uncoded and a sophisticated near-capacity-coded OFDMA/SC-FDMA STSK scheme were studied, and their performances were compared in multiuser wideband multiple-input–multiple-output (MIMO) scenarios. Explicitly, OFDMA/SC-FDMA-aided STSK exhibits an excellent performance, even in the presence of channel impairments due to the frequency selectivity of wideband channels, and proves to be a beneficial choice for high-capacity multiuser MIMO systems.**

***Index Terms*—Dispersive channel, extrinsic information transfer (EXIT) chart, orthogonal frequency division multiple access (OFDMA), single carrier frequency division multiple access (SC-FDMA), space-time shift keying (STSK).**

I. Introduction

Recently the concept of space–time shift keying (STSK) [1], [2] has been developed to provide a highly flexible diversity versus multiplexing gain tradeoff at a low decoding complexity. Multiple-input–multiple-output (MIMO) systems can attain a beneficial multiplexing gain by using, for example, BLAST or V-BLAST [3]. As a design alternative, they can also attain a diversity gain by using space–time block codes (STBCs) [4] or space–time trellis codes [5].

Manuscript received April 15, 2012; revised August 8, 2012; accepted September 16, 2012. Date of publication September 28, 2012; date of current version January 14, 2013. This work was supported in part by the Research Councils U.K. (RC-UK) through the India–U.K. Advanced Technology Centre (IU-ATC), the China–U.K. Science Bridge, and the European Union (EU) through the Concerto Project. The review of this paper was coordinated by Dr. X. Wang.

M. I. Kadir, J. Zhang, S. Chen, and L. Hanzo are with the School of ECS, University of Southampton, SO17 1BJ Southampton, U.K. (e-mail: mik1g09@ecs.soton.ac.uk; sqc@ecs.soton.ac.uk; lh@ecs.soton.ac.uk).

S. Sugiura is with the Toyota Central R&D Laboratories Inc., Nagakute, Aichi 480-1192, Japan (e-mail: sugiura@ieee.org).

Color versions of one or more of the figures in this paper are available online at http://ieeexplore.ieee.org.

Digital Object Identifier 10.1109/TVT.2012.2220794

As a further advance, linear dispersion codes were proposed [6], [7] to strike a flexible tradeoff between the achievable multiplexing and diversity gains, but at the cost of increased decoding complexity. As an additional design alternative, the concept of spatial modulation [8] emerged, which relies on using the transmit antenna index in addition to the conventional modulation constellation symbols to increase the attainable spectral efficiency. This scheme was then further developed to space shift keying (SSK) [9], which utilizes only the presence or absence of the signal energy at a specific transmit antenna for data transmission. This SSK scheme imposes an extremely low decoding complexity. Motivated by these ideas, Sugiura *et al.* conceived a low-complexity STSK design, which outperformed the family of conventional MIMO arrangements. In particular, they proposed the activation of one out of Q dispersion matrices to appropriately spread the modulated symbols, thus facilitating a low-complexity single-stream maximum-likelihood (ML) detection based on the linearized MIMO model in [7].

Although STSK-based systems have an excellent performance in narrowband channels, their performance in dispersive wireless channels may erode. To mitigate the performance degradation imposed by dispersive channels, we intrinsically amalgamated the orthogonal frequency-division multiple-access (OFDMA) and single-carrier frequency-division multiple-access (SC-FDMA) concept with the STSK system. OFDMA/SC-FDMA-aided STSK systems can attain a superb diversity–multiplexing tradeoff, even in a multipath environment, while additionally supporting multiuser transmissions and maintaining a low peak-to-average-power ratio (PAPR) in uplink (UL) SC-FDMA/STSK scenarios.

Hence, OFDMA/SC-FDMA-assisted STSK systems are advocated in this paper, because OFDMA and SC-FDMA have been adopted for the downlink (DL) and the UL of the Long Term Evolution Advanced (LTE-Advanced) standard, respectively [10]. Before transmitting the signals from each of the transmit antenna elements (AEs) of our STSK system, either the discrete Fourier transform (DFT) or the original frequency-domain (FD) symbols are mapped to a number of subcarriers, either in a contiguous subband-based fashion or by dispersing them right across the entire FD. The resulting signal is then transmitted after the inverse discrete Fourier transform (IDFT) operation.

Thus, in this paper, a novel OFDMA/SC-FDMA-aided STSK MIMO architecture is proposed, which is capable of efficient operation in frequency-selective wireless channels to strike a flexible diversity versus multiplexing gain trade-off. The transmitted signal of each subcarrier of the parallel modem experiences a nondispersive narrowband channel, and the overall STSK-based MIMO scheme exhibits a performance similar to that in narrowband channels, despite operating in a wideband scenario. The appropriate mapping of the users' symbols to subcarriers results in a flexible multiuser performance while benefitting from our low-complexity single-stream based detection. We can use a minimum mean squared error (MMSE) or zero-forcing (ZF) based single-tap MIMO FD equalizer, followed by single-stream-based detection in the TD. Furthermore, the DFT-precoding-based SC-FDMA scheme can reduce the PAPR for the mobile's UL transmissions. Finally, the performance of the proposed system that relies on a three-stage concatenated recursive systematic convolutional (RSC) and unity-rate-coding (URC) scenario is characterized through Extrinsic Information Transfer (EXIT) charts.

The remainder of this paper is organized as follows. In Section II, we present a brief overview of our proposed system, which relies on a linear dispersion-matrix-aided STSK scheme amalgamated with OFDMA/SC-FDMA transmission. In Section III, an OFDMA/SC-FDMA STSK scheme based on a three-stage RSC-URC-coded scenario is discussed. Then, the performance of the scheme, particularly of an EXIT chart aided near-capacity design is investigated in Section IV. Finally, we conclude in Section V.

Notations: In general, we use boldface letters to denote matrices or column vectors, whereas $\bullet^T$, $\bullet^H$, $\mathrm{tr}(\bullet)$, and $\| \bullet \|$ represent the transpose, the Hermitian transpose, the trace, and the Euclidean norm of the matrix "$\bullet$", respectively. The notation $\boldsymbol{a}[n_d]$ is used for the n_d-th matrix of an array of matrices $\boldsymbol{a}$, $\boldsymbol{b}_{i,j}$ for the (i,j)-th entry of the matrix $\boldsymbol{b}$; hence, $\boldsymbol{a}_{i,j}[n_d]$ represents the (i,j)-th entry of the n_d-th matrix of a matrix array $\boldsymbol{a}$. We use $vec(\bullet)$ for the column-wise vectorial stacking operation to a matrix "$\bullet$" $\in \mathbb{C}^{C\times D}$ to yield a vector $\in \mathbb{C}^{CD\times 1}$, $\mathrm{diag}\{a[0], a[1], \ldots, a[N_c-1]\}$ for a $(N_c \times N_c)$ diagonal matrix with $a[0], a[1], \ldots, a[N_c-1]$ diagonal entries, $\delta(.)$ for the Dirac delta function, $\otimes$ for the Kronecker product and $\circledast_{N_c}$ for the length-N_c circular convolution operator. The notations $\boldsymbol{\mathcal{F}}_K$ and $\boldsymbol{\mathcal{F}}_K^H$ denote the K-point DFT and IDFT matrices, respectively, and $\boldsymbol{I}_K$ indicates the $(K \times K)$-element identity matrix. Furthermore, the generalized user is represented by u, whereas user u' refers to the desired user.

II. System Overview

We consider an OFDMA/SC-FDMA STSK system with M transmit and N receive AEs. The channel is assumed to be a frequency-selective Rayleigh fading medium, which can be modeled by a finite impulse response filter with time-varying tap values [11], [12]. In our investigations of the system performance in Section IV, we have utilized the COST207-TU12 channel specifications for the delay and the Doppler power spectral density to represent a typical urban scenario. The number of subcarriers employed for the transmission of N_d STSK blocks of a single user after N_d-point DFT processing is N_c.

A. Transmitter

The transceiver architecture of our OFDMA/SC-FDMA STSK system is shown in Fig. 1. The signals are transmitted from different transmit AEs within T different symbol intervals after being mapped by the space–time (ST) mapper of the STSK block and after OFDMA/SC-FDMA-based processing. To be specific, the STSK encoder in Fig. 1 maps the source information of one of the U users to ST blocks $\boldsymbol{x}^u[n_d] \in \mathbb{C}^{M\times T}$, $n_d = 0, 1, \ldots, (N_d-1)$ according to [2]

$$\boldsymbol{x}^u[n_d] = s^u[n_d]\boldsymbol{A}^u[n_d] \quad u = 0, 1, \ldots (U-1) \tag{1}$$

where $s^u[n_d]$ and $\boldsymbol{A}^u[n_d]$ represent the uth user's $\mathcal{L}$–ary phase-shift keying (PSK)/quadrature amplitude modulation (QAM) symbol and activated dispersion matrix (DM), respectively, from a set of Q such matrices $\boldsymbol{A}_q$ $(q = 1, 2. \ldots, Q)$, which are preassigned in advance of transmissions. The DMs may be generated, for example, either by maximizing the continuous-input–continuous-output memoryless channel capacity or the discrete-input–continuous-output memoryless channel capacity or, alternatively, by minimizing the maximum pairwise symbol error probability (PSEP) under the power-constraint criterion [7], [13] of

$$\mathrm{tr}\left(\boldsymbol{A}_q^H \boldsymbol{A}_q\right) = T \qquad \forall q. \tag{2}$$

Thus, a block of $\log_2(\mathcal{L}\cdot Q)$ number of bits are transmitted by the ST mapper in Fig. 1 per symbol interval, which forms an STSK ST block, and the STSK system in Fig. 1 is uniquely specified by the parameters (M, N, T, Q) in conjunction with the $\mathcal{L}$-PSK or $\mathcal{L}$-QAM scheme, where N is the number of receiver AEs.

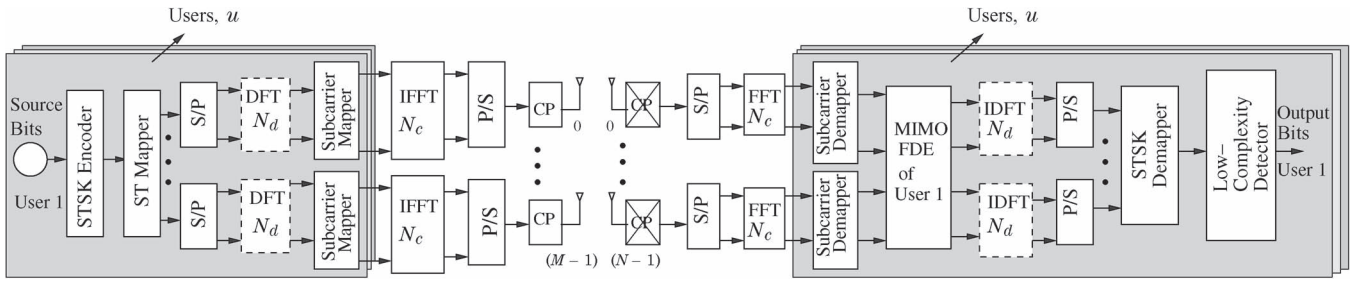

Fig. 1. Transmission model of the SC-FDMA-aided STSK scheme. In the OFDMA-aided scheme, the dotted blocks "DFT N_d" in the transmitter and "IDFT N_d" in the receiver do not exist. The STSK mapper selects one out of the Q dispersion matrices along with one constellation symbol, and the resulting space–time codewords are passed in different time slots through the OFDMA- or SC-FDMA-based multiuser transmission system before being transmitted through the transmit AEs. Because a single dispersion matrix is selected in one transmission block, a low-complexity single-stream ML detector can be employed.

After generating the ST blocks $\boldsymbol{x}^u[n_d]$ for a particular user u, we employ frame-based transmission. In particular, N_c subcarriers are used for transmitting a frame, each frame consisting of N_d STSK blocks. To be specific, we define the transmit frame $\tilde{\boldsymbol{x}}^u \in \mathbb{C}^{MN_d \times T}$ for user u as

$$\tilde{\boldsymbol{x}}^u = \begin{bmatrix} \tilde{\boldsymbol{x}}^u_{0,0} & \tilde{\boldsymbol{x}}^u_{0,1} & \cdots & \tilde{\boldsymbol{x}}^u_{0,(T-1)} \\ \tilde{\boldsymbol{x}}^u_{1,0} & \tilde{\boldsymbol{x}}^u_{1,1} & \cdots & \tilde{\boldsymbol{x}}^u_{1,(T-1)} \\ \vdots & \vdots & \ddots & \vdots \\ \tilde{\boldsymbol{x}}^u_{(M-1),0} & \tilde{\boldsymbol{x}}^u_{(M-1),1} & \cdots & \tilde{\boldsymbol{x}}^u_{(M-1),(T-1)} \end{bmatrix} \tag{3}$$

where each $(N_d \times 1)$-element data vector $\tilde{\boldsymbol{x}}^u_{m,T_i}$, $m = 0, 1, \ldots, (M-1)$ $T_i = 0, 1, \ldots, (T-1)$ can be represented by

$$\tilde{\boldsymbol{x}}^u_{m,T_i} = \left[\boldsymbol{x}^u_{m,T_i}[0], \boldsymbol{x}^u_{m,T_i}[1], \ldots, \boldsymbol{x}^u_{m,T_i}[N_d-1]\right]^T \tag{4}$$

which undergoes the N_d-point DFT operation.

To expound a little further, the data stream $\tilde{\boldsymbol{x}}^u_{m,T_i}$ to be transmitted from the transmit AE m at a specific time interval T_i is first DFT precoded by the N_d-point DFT block; in case of OFDMA, however, this step is not required. Then, assuming a full-load system, the FD symbols $\boldsymbol{X}_{m,T_i} \in \mathbb{C}^{N_d \times 1}$ output from the N_d-point DFT block of the SC-FDMA STSK scheme (or the direct FD STSK codeword symbols of the OFDMA STSK scheme) are mapped to N_c subcarriers with $N_c = (N_d \times U)$, where the subcarrier allocation may be in contiguous [localized frequency-division multiple-access (LFDMA)] [14] or an interleaved [interleaved frequency-division multiple-access (IFDMA)] [14] fashion. Denoting the set of subcarriers allocated to user u by $\mathcal{S}_u$, the subcarrier allocation matrix $\boldsymbol{P}^u \in \mathbb{C}^{N_c \times N_d}$ may be represented by [15]

$$\boldsymbol{P}^u_{n_c,n_d} = \begin{cases} 1, & \text{if } n_c \in \mathcal{S}_u \text{ and subcarrier } n_c \\ & \text{is allocated to } \boldsymbol{\mathcal{F}}_{N_d}\mathbf{x}^u_{m,T_i}[n_d] \\ 0, & \text{otherwise} \end{cases} \tag{5}$$

where we have

$$n_c = \begin{cases} (n_d \times U) + u, & IFDMA \\ (N_d \times u) + n_d, & LFDMA \end{cases} \tag{6}$$

for all $n_c = 0, 1, \ldots, (N_c - 1)$ and all $n_d = 0, 1, \ldots, (N_d - 1)$.

Defining $\boldsymbol{C}_{add}(\bullet)$ as a matrix [16] that adds a TD cyclic prefix (CP) of length L_{cp} (which is higher than the channel's delay spread) to the N_c-length vector $(\bullet)$, the TD data vector after the IDFT operation may be written as

$$\breve{\boldsymbol{x}}^u_{m,T_i} = \boldsymbol{C}_{add}\left(\boldsymbol{\mathcal{F}}^H_{N_c}\boldsymbol{P}^u\boldsymbol{\mathcal{F}}_{N_d}\boldsymbol{x}^u_{m,T_i}\right) \tag{7}$$

$$= \boldsymbol{C}_{add}\left(\boldsymbol{\mathcal{F}}^H_{N_c}\boldsymbol{P}^u\boldsymbol{X}_{m,T_i}\right). \tag{8}$$

Hence, the uth user's transmit frame after IDFT operation can be formulated in a similar form as (3), yielding

$$\breve{\boldsymbol{x}}^u = \begin{bmatrix} \breve{\boldsymbol{x}}^u_{0,0} & \breve{\boldsymbol{x}}^u_{0,1} & \cdots & \breve{\boldsymbol{x}}^u_{0,(T-1)} \\ \breve{\boldsymbol{x}}^u_{1,0} & \breve{\boldsymbol{x}}^u_{1,1} & \cdots & \breve{\boldsymbol{x}}^u_{1,(T-1)} \\ \vdots & \vdots & \ddots & \vdots \\ \breve{\boldsymbol{x}}^u_{(M-1),0} & \breve{\boldsymbol{x}}^u_{(M-1),1} & \cdots & \breve{\boldsymbol{x}}^u_{(M-1),(T-1)} \end{bmatrix} \tag{9}$$

where each vector $\breve{\boldsymbol{x}}^u_{m,T_i}$ is defined by (7) and (8) with

$$\breve{\boldsymbol{x}}^u_{m,T_i} \in \mathbb{C}^{(N_c+L_{cp})\times 1} \tag{10}$$

and hence

$$\breve{\boldsymbol{x}}^u \in \mathbb{C}^{(N_c+L_{cp})M \times T}. \tag{11}$$

Each link of the M transmit and N receive AE-aided system is assumed to be frequency selective, whose channel impulse response (CIR) may be modeled as the ensemble of all the propagation paths [11], [12], i.e.,

$$h^u_{n,m}(t,\tau) = \sum_{l=0}^{(L-1)} a^u_l g^u_l(t)\delta\left(\tau - \tau^u_l\right) \tag{12}$$

for each $n = 0, 1, \ldots, (N-1)$, $m = 0, 1, \ldots, (M-1)$, and $u = 0, 1, \ldots (U-1)$. Here, L is the number of multipath components in the channel between the mth transmit and the nth receive AE, and a^u_l, τ^u_l, and $g^u_l(t)$ are the channel's envelope, delay, and Rayleigh fading process that exhibits a particular normalized Doppler frequency f_d, respectively, associated with the lth path of user u.

Note that we use h and $\boldsymbol{H}$ to denote the CIR and the $(N \times M)$-element CIR matrix, respectively, whereas $\tilde{h}$ and $\tilde{\boldsymbol{H}}$ denote the channel's frequency-domain channel transfer function (FDCHTF) and the $(N \times M)$-element frequency-domain channel transfer matrix (FDCHTM), respectively.

B. Receiver

Assuming perfect synchronization at the receiver in Fig. 1 and after removing the CP, the discrete-time input to the receiver's "N_c-point IDFT" block at the receive AE n at time slot T_i is given by [17]

$$\boldsymbol{y}_{n,T_i} = \sum_{u=0}^{(U-1)}\sum_{m=0}^{(M-1)} \boldsymbol{h}^u_{n,m} \circledast_{N_c} \breve{\boldsymbol{x}}^u_{m,T_i} + \mathbf{v}_{n,T_i} \tag{13}$$

where $\circledast_{N_c}$ represents the length-N_c circular convolution operator, and $\boldsymbol{v}_{n,T_i}$ is the noise vector.

Defining the FDCHTM by $\tilde{\boldsymbol{H}}^{u}$, the FD transmit codeword matrix after subcarrier mapping by $\tilde{\boldsymbol{X}}^{u}$ and the FD additive white Gaussian noise (AWGN) matrix by $\boldsymbol{V}$, the FD output matrix $\boldsymbol{Y}$ after the N_c-point DFT of our ST architecture may be written as

$$\boldsymbol{Y} = \sum_{u=0}^{(U-1)} \tilde{\boldsymbol{H}}^{u} \tilde{\boldsymbol{X}}^{u} + \boldsymbol{V} \tag{14}$$

where each (n, m)-th component of $\tilde{\boldsymbol{H}}^{u}$ is formulated as

$$\tilde{\boldsymbol{H}}^{u}_{n,m} = \text{diag}\left\{\tilde{h}^{u}_{n,m}[0], \tilde{h}^{u}_{n,m}[1], \ldots, \tilde{h}^{u}_{n,m}[N_c - 1]\right\} \in \mathbb{C}^{N_c \times N_c} \tag{15}$$

where $\tilde{h}^{u}_{n,m}$ denotes the FDCHTF that corresponds to user u, and the components of $\tilde{\boldsymbol{X}}^{u}$, $\boldsymbol{V}$, and $\boldsymbol{Y}$ are defined by

$$\tilde{\boldsymbol{X}}^{u}_{m,T_i} = \boldsymbol{P}^{u} \boldsymbol{X}^{u}_{m,T_i} \in \mathbb{C}^{N_c \times 1} \tag{16}$$

$$\boldsymbol{V}_{n,T_i} \in \mathbb{C}^{N_c \times 1} \tag{17}$$

$$\boldsymbol{Y}_{n,T_i} \in \mathbb{C}^{N_c \times 1}. \tag{18}$$

Hence, the components of $\boldsymbol{Y}$ can be formulated based on (14) as

$$\boldsymbol{Y}_{n,T_i} = \sum_{u=0}^{U-1} \tilde{\boldsymbol{H}}^{u}_{n,m} \boldsymbol{P}^{u} \boldsymbol{X}^{u}_{m,T_i} + \boldsymbol{V}_{n,T_i} \tag{19}$$

$$= \sum_{u=0}^{U-1} \tilde{\boldsymbol{H}}^{u}_{n,m} \boldsymbol{P}^{u} \boldsymbol{\mathcal{F}}_{N_d} \tilde{\boldsymbol{x}}^{u}_{m,T_i} + \boldsymbol{V}_{n,T_i}. \tag{20}$$

Now, after subcarrier demapping and MIMO frequency-domain equalization (FDE), the received symbols are passed through the "N_d-point IDFT" block of user u'. Defining $\tilde{\boldsymbol{P}}^{u} = [\boldsymbol{P}^{u}]^{T}$ as the subcarrier demapping matrix and $\boldsymbol{W}^{u'}$ as the weight matrix of the MIMO ZF or MMSE FDE of user u', which is given by [18]

$$\boldsymbol{W}^{u'} = \begin{cases} \left[(\tilde{\boldsymbol{H}}^{u'})^{H} \tilde{\boldsymbol{H}}^{u'}\right]^{-1} (\tilde{\boldsymbol{H}}^{u'})^{H} & \text{ZF} \\ \left[(\tilde{\boldsymbol{H}}^{u'})^{H} \tilde{\boldsymbol{H}}^{u'} + \sigma_N^2 \boldsymbol{I}_M\right]^{-1} (\tilde{\boldsymbol{H}}^{u'})^{H} & \text{MMSE} \end{cases} \tag{21}$$

where σ_N^2 denotes the variance of the additive noise, the elements of the TD output $\boldsymbol{z}^{u'}$ of user u' after the IDFT operation may be expressed as [15]

$$\boldsymbol{z}^{u'}_{m,T_i} = \boldsymbol{\mathcal{F}}^{H}_{N_d} \tilde{\boldsymbol{P}}^{u'} \boldsymbol{W}^{u'}_{m,n} \times \left(\tilde{\boldsymbol{H}}^{u'}_{n,m} \boldsymbol{P}^{u'} \boldsymbol{\mathcal{F}}_{N_d} \tilde{\boldsymbol{x}}^{u'}_{m,T_i} + \sum_{\substack{u=0 \\ u \neq u'}}^{U-1} \tilde{\boldsymbol{H}}^{u}_{n,m} \boldsymbol{P}^{u} \boldsymbol{\mathcal{F}}_{N_d} \tilde{\boldsymbol{x}}^{u}_{m,T_i} \right) + \tilde{\boldsymbol{v}}^{u'}_{m,T_i} \tag{22}$$

where $\boldsymbol{z}^{u'}_{m,T_i}$ and $\boldsymbol{W}^{u'}_{m,n}$ are the (m, T_i)-th and (m, n)-th components of $\boldsymbol{z}^{u'}$ and $\boldsymbol{W}^{u'}$, respectively. Because each $\tilde{\boldsymbol{H}}^{u}_{n,m}$ is diagonal, we see based on (21) that each $\boldsymbol{W}^{u'}_{m,n}$ will also be diagonal. Due to the diagonal nature of both $\tilde{\boldsymbol{H}}^{u}_{n,m}$ and $\boldsymbol{W}^{u'}_{m,n}$ and because

$$\tilde{\boldsymbol{P}}^{u} \boldsymbol{P}^{u} = \begin{cases} \boldsymbol{I}_{N_d}, & u = u' \\ 0, & u \neq u' \end{cases} \tag{23}$$

we have

$$\boldsymbol{z}^{u'}_{m,T_i} = \boldsymbol{\mathcal{F}}^{H}_{N_d} \tilde{\boldsymbol{P}}^{u'} \boldsymbol{W}^{u'}_{m,n} \tilde{\boldsymbol{H}}^{u'}_{n,m} \boldsymbol{P}^{u'} \boldsymbol{\mathcal{F}}_{N_d} \tilde{\boldsymbol{x}}^{u'}_{m,T_i} + \tilde{\boldsymbol{v}}^{u'}_{m,T_i}. \tag{24}$$

Based on (24), observe that, under the idealized assumption of perfect synchronization, perfect orthogonality of the users using different subcarriers and by exploiting the perfectly diagonal nature of both $\boldsymbol{W}^{u'}_{m,n}$ and of the FDCHTMs $\tilde{\boldsymbol{H}}^{u'}_{n,m}$, our scheme becomes free from multiuser interferences (MUIs). However, the symbols that are transmitted by a given user in the context of both the LFDMA and IFDMA schemes with MMSE equalization will experience some form of self-interference (SI) [15]. By contrast, the ZF scheme can completely mitigate the SI and the DFT matrices $\boldsymbol{\mathcal{F}}^{H}_{N_d}$ and $\boldsymbol{\mathcal{F}}_{N_d}$, the subcarrier mapping and demapping matrices, $\boldsymbol{P}^{u'}$ and $\tilde{\boldsymbol{P}}^{u'}$, and the FDCHTM $\tilde{\boldsymbol{H}}^{u'}$, and the MMSE equalization matrix $\boldsymbol{W}^{u'}$ is absent in (24), although the scheme suffers from performance degradation due to the inherent noise enhancement process when a particular subcarrier experiences deep fading. Hence, following the FD equalization and the receiver's IDFT operation in Fig. 1, the decision variable $\boldsymbol{z}^{u'}$ for the ZF scheme can readily be written as

$$\boldsymbol{z}^{u'}[n_d] = \tilde{\boldsymbol{x}}^{u'}[n_d] + \tilde{\boldsymbol{v}}^{u'}[n_d] \tag{25}$$

where $\tilde{\boldsymbol{x}}^{u'}[n_d] \in \mathbb{C}^{M \times T}$, and $\tilde{\boldsymbol{v}}^{u'}[n_d] \in \mathbb{C}^{M \times T}$ for all $n_d = 0, 1, \ldots, (N_d - 1)$.

The IFDMA principle, on the other hand, increases the FD separation between the subcarriers and thereby provides some additional diversity gain. Thus, the decision variable of our scheme using ZF or assuming the mitigation of MMSE SI may be formulated, using the linearized sytem model in [7], as

$$\overline{\boldsymbol{z}}^{u'}[n_d] = \boldsymbol{\chi} \boldsymbol{k}^{u'} + \bar{\mathbf{v}}^{u'}[n_d] \tag{26}$$

where $\overline{\boldsymbol{z}}^{u'}[n_d]$ is the $(MT \times 1)$-element matrix that was obtained by applying the vectorial stacking operation $vec(\cdot)$ to the received FD signal block $\boldsymbol{z}^{u'}[n_d]$, whereas $\boldsymbol{\chi} = [vec(\boldsymbol{A}_1) \ldots vec(\boldsymbol{A}_Q)] \in \mathbb{C}^{MT \times Q}$ is the dispersion character matrix [13], and, finally, $\bar{\boldsymbol{v}}^{u'}[n_d] = vec(\tilde{\boldsymbol{v}}^{u'}[n_d]) \in \mathbb{C}^{MT \times 1}$ is the stacked AWGN vector. Still referring to (26), the equivalent transmit signal vector is represented by

$$\boldsymbol{k}^{u'} = [0, \ldots, 0, s^{u'}, 0, \ldots, 0]^{T} \in \mathbb{C}^{Q \times 1} \tag{27}$$

where $(q - 1)$ and $(Q - q)$ numbers of zeros surround the $\mathcal{L}$-PSK or $\mathcal{L}$-QAM symbol $s^{u'}$ in the u'-th user's equivalent transmit signal vector $\boldsymbol{k}^{u'}$, and the symbol $s^{u'}$ is exactly located at the qth position, where q is the index of the activated DM.

We can now employ the single-stream-based ML detection [2] to detect the indices q and l_c of the DM activated and the constellation symbol used, respectively. The estimates $(\hat{q}, \hat{l}_c)$ can be determined from

$$(\hat{q}, \hat{l}_c) = \arg\min_{q, l_c} \left\| \overline{\boldsymbol{z}}^{u'}[n_d] - \boldsymbol{\chi} \boldsymbol{k}^{u'}_{q,l_c} \right\|^2 \tag{28}$$

$$= \arg\min_{q, l_c} \left\| \overline{\boldsymbol{z}}^{u'}[n_d] - (\boldsymbol{\chi})_q (s^{u'})_{l_c} \right\|^2 \tag{29}$$

where $(s^{u'})_{l_c}$ is the l_c-th $\mathcal{L}$-PSK or the $\mathcal{L}$-QAM symbol, $(\boldsymbol{\chi})_q$ represents the qth column of $\boldsymbol{\chi}$, and $\boldsymbol{k}^{u'}_{q,l_c}$ is the equivalent transmit signal vector in (27) that corresponds to user u' at indices q and l_c.

In case of OFDMA, we have, $\boldsymbol{\mathcal{F}}^{H}_{N_d} = \boldsymbol{\mathcal{F}}_{N_d} = \boldsymbol{I}_{N_d}$. In other words, the blocks "N_d-point DFT" and "N_d-point IDFT" do not exist in OFDMA, and as such, the OFDMA scheme cannot benefit from the potential diversity provided by the DFT-based precoding stage. We can thus proceed with our ZF or MMSE weight matrix $\boldsymbol{W}^{u'}$ as aforementioned. Alternatively, for the OFDMA STSK, the ML detector of [2] can directly be applied in the FD without employing

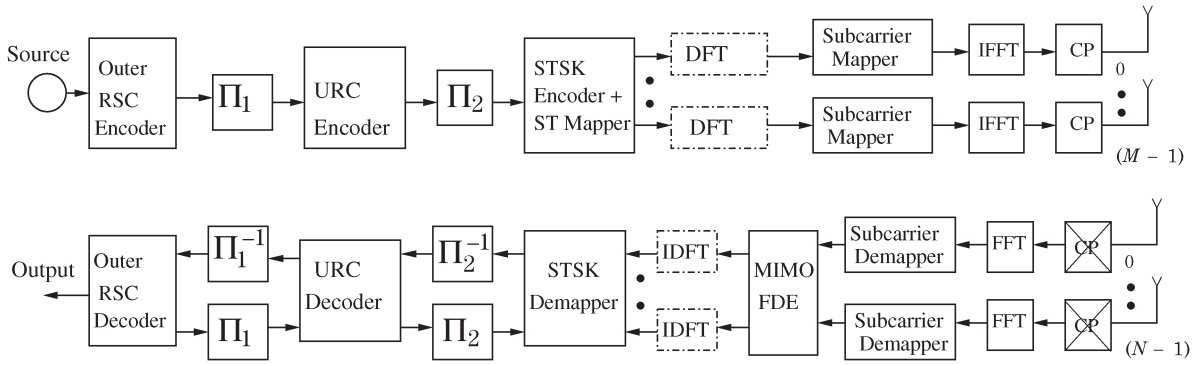

Fig. 2. Three-stage RSC-URC-coded OFDMA/SC-FDMA STSK transceiver. The dotted "DFT" block in the transmitter and the "IDFT" block in the receiver do not appear in the coded OFDMA STSK.

the MIMO FDE. To be specific, in the absence of the weight matrix $\boldsymbol{W}^{u'}$ and with the substitution $\boldsymbol{\mathcal{F}}_{N_d}^H = \boldsymbol{\mathcal{F}}_{N_d} = \boldsymbol{I}_{N_d}$, (24) reduces to $\boldsymbol{Z}_{m,T_i}^{u'} = \tilde{\boldsymbol{H}}_{n,m}^{u'} \tilde{\boldsymbol{x}}_{m,T_i}^{u'} + \tilde{\boldsymbol{v}}_{m,T_i}^{u'}$, where $\boldsymbol{z}_{m,T_i}^{u'}$ is replaced by $\boldsymbol{Z}_{m,T_i}^{u'}$ when the MIMO FDE is not employed. The direct ML detector of [2] for the OFDMA STSK scheme can thus be formulated as

$$(\hat{q}, \hat{l}_c) = \arg\min_{q,l_c} \left\| \overline{\boldsymbol{Z}}^{u'}[n_d] - \left(\overline{\tilde{\boldsymbol{H}}}^{u'}[n_d] \boldsymbol{\chi} \right)_q (s^{u'})_{l_c} \right\|^2 \tag{30}$$

where $\overline{\boldsymbol{Z}}^{u'}[n_d] = vec(\boldsymbol{Z}^{u'}[n_d])$, and the equivalent FDCHTM $\overline{\tilde{\boldsymbol{H}}}^{u'}[n_d]$ is given by $\overline{\tilde{\boldsymbol{H}}}^{u'}[n_d] = \boldsymbol{I}_T \otimes \tilde{\boldsymbol{H}}^{u'}[n_d]$, whereas other notations are as used in (29).

In addition, we can see that our OFDMA/SC-FDMA STSK signal can be detected from (29) at a low complexity, because of the following two reasons.

1) Equation (29) does not explicitly contain either the FD channel transfer function or the TD CIR. Hence, data estimation using this equation involves a reduced number of multiplications and additions.
2) We can successfully employ the single-stream-based ML detection that relies on the linearized model in [7], because only a single DM is activated at a given STSK block interval.

III. Channel-Coded OFDMA/SC-FDMA STSK

In this section, we investigate the three-stage parallel concatenated RSC-coded OFDMA/SC-FDMA STSK scheme in Fig. 2. The source bits are first convolutionally encoded and then interleaved by a random bit interleaver Π_1. A (2, 1, 2) RSC code is employed, and following channel interleaving, the symbols are precoded by a URC scheme, which was shown to be beneficial, because it efficiently spreads the extrinsic information as a benefit of its infinite impulse response [13]. Then, the precoded bits are further interleaved by a second interleaver Π_2 in Fig. 2, and the interleaved bits are then transmitted by the OFDMA/SC-FDMA STSK scheme in the TD using an M-element MIMO transmitter.

As shown at the receiver in Fig. 2, after removing the CP, the received symbols are passed through the FFT unit, and the resulting FD symbols are then deallocated in an inverse fashion according to the IFDMA/LFDMA scheme used. The demapped symbols of a user are then equalized by the MIMO FDE, passed through another IDFT unit in Fig. 2 in accordance with the DFT precoding used, before they are then fed to the STSK demapper. We note that the equivalent received signal $\overline{\boldsymbol{z}}^{u'}$ carries $B^{u'}$ channel-coded bits $b^{u'} = [b_1^{u'}, b_2^{u'}, \ldots, b_B^{u'}]$, and the extrinsic log-likelihood ratio (LLR) of $b_k^{u'}$, $k = 1, \ldots, B^{u'}$ can be expressed as [13]

$$L_e\left(b_k^{u'}\right) = \ln \frac{\sum_{\boldsymbol{k}_{q,l_c}^{u'}} \epsilon \boldsymbol{k}_1^{u'} e^{-\left\| \overline{\boldsymbol{z}}^{u'} - \boldsymbol{\chi} \boldsymbol{k}_{q,l_c}^{u'} \right\|^2 / N_0 + \sum_{j \neq k} b_j^{u'} L_a\left(b_j^{u'}\right)}}{\sum_{\boldsymbol{k}_{q,l_c}^{u'}} \epsilon \boldsymbol{k}_0^{u'} e^{-\left\| \overline{\boldsymbol{z}}^{u'} - \boldsymbol{\chi} \boldsymbol{k}_{q,l_c}^{u'} \right\|^2 / N_0 + \sum_{j \neq k} b_j^{u'} L_a\left(b_j^{u'}\right)}} \tag{31}$$

where $L_a(\bullet)$ denotes the *a priori* LLR of the bits that correspond to "$\bullet$," and $\boldsymbol{k}_1^{u'}$ and $\boldsymbol{k}_0^{u'}$ refer to the sets of the possible equivalent transmit signal vectors $\boldsymbol{k}^{u'}$ of user u' when $b_k^{u'} = 1$ and $b_k^{u'} = 0$, respectively.

Then, the URC decoder in Fig. 2 processes the information provided by the STSK demapper, in conjunction with the *a priori* information, to generate the *a posteriori* probability. The URC generates extrinsic information for both the RSC decoder and the demapper in Fig. 2. The RSC channel decoder, which can be called the external decoder, exchanges extrinsic information with the URC decoder and, after a number of iterations, outputs the estimated bits. It is noteworthy here that, for each of the outer iterations between the RSC decoder and the URC, there are a number of inner iterations between the URC and the STSK demapper.

IV. Performance of the Proposed Scheme

We have investigated both the OFDMA-DL-and the SC-FDMA-aided UL STSK schemes for both the IFDMA and LFDMA algorithms using the simulation parameters in Table I.

Observe in Fig. 3 that the SC-FDMA STSK scheme that employs MMSE equalization operating in an uncoded scenario exhibits better bit-error rate (BER) performance than that of OFDMA STSK, which is a benefit of the additional FD diversity attained by the DFT-precoding in Fig. 1. The performance of IFDMA is shown to be better than the LFDMA due to the higher FD separation between the subcarriers of the same user, which hence results in independent FD fading. The multiuser performance[1] attained is also investigated and is more or less similar to the single-user scenario due to the absence of MUI because of the diagonal nature of the weight matrix $\boldsymbol{W}_{m,n}^{u'}$ in (24). Furthermore, in Fig. 3, observe that SC-FDMA STSK exhibits better performance than OFDMA STSK in both the LFDMA and IFDMA regimes that employ MMSE-based FD equalization and ML detection. The achievable performance is, however, degraded, when ZF is used due to the noise enhancement imposed. The performance of the

[1]The multiuser performance curves for the uncoded scenario, however, are not included here for space economy.

TABLE I
MAIN SIMULATION PARAMETERS

Simulation parameter	*Value*
Fast fading model	Corr. Rayleigh fading
Normalized Doppler frequency, f_d	0.01
Channel specification	COST207-TU12
No. of subcarriers	64
N_d-point DFT precoder	16
Length of cyclic prefix	32
No. of Tx AE, M	2
No. of Rx AE, N	2
No. of Tx time slots, T	2
No. of dispersion matrices	$Q = 2, 4$
STSK specification	$(2, 2, 2, Q)$, $Q = 2, 4$
Modulation order	2
Outer decoder	RSC $(2, 1, 2)$
Generator polynomials	$(g_r, g) = (3, 2)_8$
Size of interleavers	4608000 bits
Outer decoding iterations	9
Inner decoder	URC
Inner decoding iterations	2

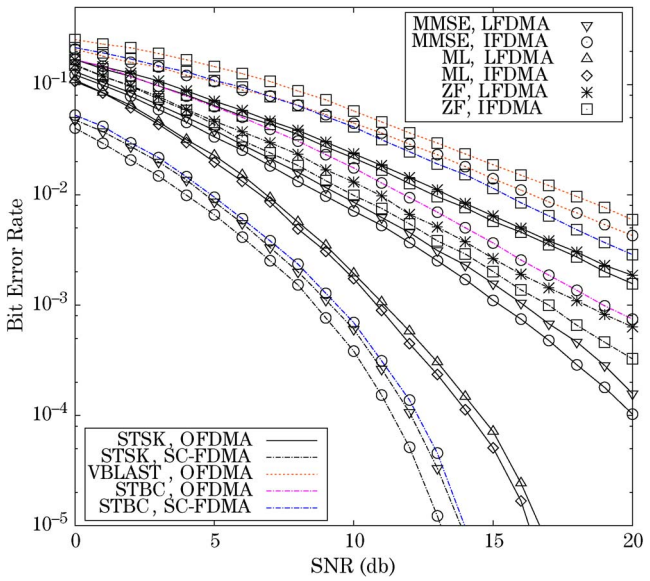

Fig. 3. Performance of the single-user OFDMA/SC-FDMA STSK (2, 2, 2, 2) system with BPSK modulation in a dispersive COST207-TU12 channel with different allocation schemes, ZF and MMSE FDE, and the ML detector of [2]. The performance of the scheme is also compared to V-BLAST $(M, N) = (2, 2)$, OFDMA, BPSK, $\mathcal{G}_2$-STBC $(M, N) = (2, 2)$, OFDMA/SC-FDMA, and BPSK benchmarker under the same channel condition.

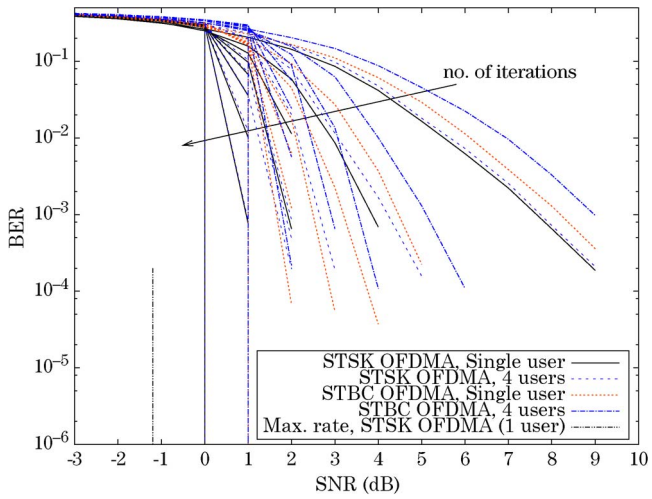

Fig. 4. BER performance of our channel-coded MMSE equalization-based OFDMA STSK (2, 2, 2, 2) that employs BPSK modulation in the dispersive COST207-TU12 channel and the corresponding $\mathcal{G}_2$-STBC scheme. The maximum achievable rate for the corresponding scheme for a single user, computed using the EXIT chart's area property, is also shown.

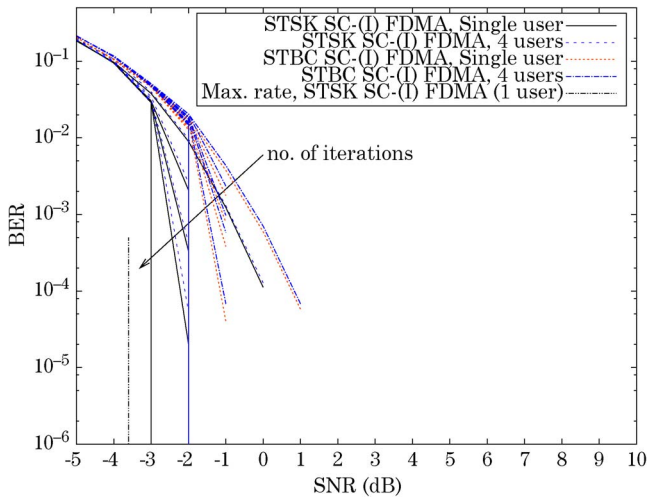

Fig. 5. Achievable BER performance of our channel-coded MMSE-based SC-FDMA STSK (2, 2, 2, 2) with BPSK modulation in the COST207-TU12 channel and the corresponding $\mathcal{G}_2$-STBC scheme with similar parameters. The maximum achievable rate of the corresponding scheme with a single user is also shown.

proposed STSK-based scheme is also compared to those of the V-BLAST-aided [3] and $\mathcal{G}_2$-STBC-aided [4], [19] OFDMA/SC-FDMA schemes using the same number of transmit and receive AEs (M, N) and the same throughput per block interval in Fig. 3, which demonstrates the efficacy of the proposed scheme.

In Figs. 4 and 5, we also characterized the achievable BER performance of the three-stage RSC- and URC-coded OFDMA/SC-FDMA STSK (2, 2, 2, 2) binary phase-shift keying (BPSK) scheme that relies on interleaved subcarrier allocation strategy in the context of the wideband COST207-TU12 channel [11], where we employed a half-rate RSC code with a constraint length of $k_c = 2$ and the octrally represented generator polynomials of $(g_r, g) = (3, 2)_8$, as well as two random interleavers with a memory of 4 608 000 b. The numbers of inner and outer decoder iterations were set to $I_{inner} = 2$ and $I_{outer} = 9$, respectively. We also investigated the performance of the SC-LFDMA scheme, and the performance was observed to be similar to SC-IFDMA in the coded scenario. (However, the SC-LFDMA performance figure has not been included here to limit the total number of figures.) The performance of both the OFDMA STSK and SC-(I)FDMA STSK has been compared to the corresponding $\mathcal{G}_2$-STBC benchmarkers. The maximum achievable rates of our schemes were also calculated by exploiting the so-called area property of EXIT charts. To be specific, it was shown in [20]–[22] that the area under the inner decoder's EXIT curve at a certain signal-to-noise ratio (SNR) quantifies the maximum achievable rate of the system, where an infinitesimally low BER may be achieved. The SNRs that correspond to the maximum achievable rates of the schemes are also shown in Figs. 4 and 5.

Fig. 6 portrays the EXIT chart of the SC-FDMA STSK(2, 2, 2, 4) arrangement combined with QPSK modulation and the IFDMA strategy, where the SNR was varied from -5 dB to 1 dB in steps of 0.5 dB. It is shown that an open EXIT tunnel is formed at SNR $= -4.0$ dB using an interleaver depth of 4 608 000 b. The corresponding staircase-shaped decoding trajectory [22] based on bit-by-bit Monte

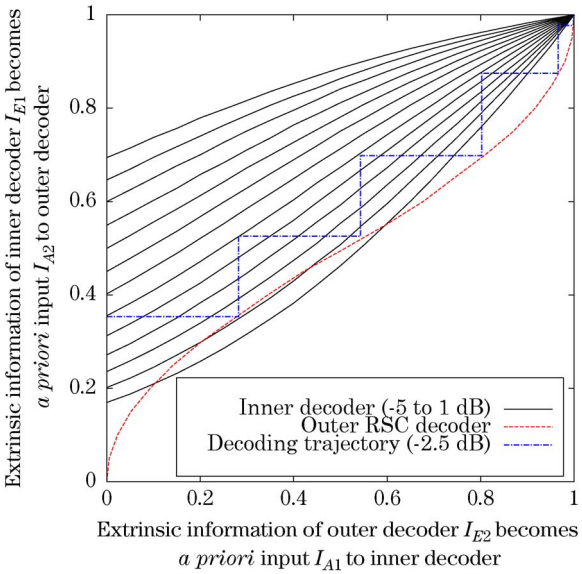

Fig. 6. EXIT trajectory of our three-stage turbo-detected MMSE-based SC-(I)FDMA STSK(2, 2, 2, 4) with QPSK modulation applied in a COST207-TU12 dispersive channel model with $f_d = 0.01$. The EXIT trajectory at -2.5 dB is mapped on inner decoder EXIT curves from -5 to 1 dB in steps of 0.5 dB and the outer RSC decoder EXIT function.

Carlo simulations conducted at -2.5 dB is also shown. Thus, it can be inferred that an infinitesimally low BER may be achieved at SNR $= -2.5$ dB in a UL scenario after $I_{outer} = 5$ iterations.

V. Conclusion

In this paper, an OFDMA/SC-FDMA aided STSK scheme has been proposed, which overcomes the impairments of realistic dispersive channels while facilitating multiuser transmissions. The scheme benefits from the flexible diversity versus multiplexing gain tradeoff offered by the recently developed STSK scheme that relies on low-complexity single-stream-based ML detection. We quantified the relative merits of OFDMA and SC-FDMA when combined with STSK and advocated the SC-FDMA-based STSK scheme that relies on the interleaved subcarrier allocation in the UL scenario as a benefit of its low PAPR. The effects of the spatial correlation between the different AEs of a multiple antenna UL, however, have to further be investigated and will be included in our future study.

It is worth mentioning here that the dispersion matrices invoked for constructing our STSK system were optimized by an exhaustive search to minimize the maximum PSEP under the power constraint in (2). However, instead of using an exhaustive search method, a heuristic- or genetic-algorithm-aided optimization of the dispersion matrices [23]–[25] may also be investigated.

The EXIT charts of the proposed scheme converge to the (1.0, 1.0) point of perfect convergence to a vanishingly low BER after a few iterations, thus indicating a sharp decrease of the BER curve.

References

[1] S. Sugiura, S. Chen, and L. Hanzo, "A universal space–time architecture for multiple-antenna-aided systems," *IEEE Commun. Surveys Tuts.*, vol. 14, no. 2, pp. 401–420, Jan. 2012.

[2] S. Sugiura, S. Chen, and L. Hanzo, "Coherent and differential space–time shift keying: A dispersion matrix approach," *IEEE Trans. Commun.*, vol. 58, no. 11, pp. 3219–3230, Nov. 2010.

[3] G. Foschini, G. Golden, R. Valenzuela, and P. Wolniansky, "Simplified processing for high spectral efficiency wireless communication employing multielement arrays," *IEEE J. Sel. Areas Commun.*, vol. 17, no. 11, pp. 1841–1852, Nov. 1999.

[4] V. Tarokh, H. Jafarkhani, and A. Calderbank, "Space–time block codes from orthogonal designs," *IEEE Trans. Inf. Theory*, vol. 45, no. 5, pp. 1456–1467, Jul. 1999.

[5] V. Tarokh, N. Seshadri, and A. Calderbank, "Space–time codes for high-data-rate wireless communication: Performance criterion and code construction," *IEEE Trans. Inf. Theory*, vol. 44, no. 2, pp. 744–765, Mar. 1998.

[6] B. Hassibi and B. M. Hochwald, "High-rate codes that are linear in space and time," *IEEE Trans. Inf. Theory*, vol. 48, no. 7, pp. 1804–1824, Jul. 2002.

[7] R. W. Heath, Jr. and A. Paulraj, "Linear dispersion codes for MIMO systems based on frame theory," *IEEE Trans. Signal Process.*, vol. 50, no. 10, pp. 2429–2441, Oct. 2002.

[8] R. Mesleh, H. Haas, S. Sinanovic, C. W. Ahn, and S. Yun, "Spatial modulation," *IEEE Trans. Veh. Technol.*, vol. 57, no. 4, pp. 2228–2241, Jul. 2008.

[9] J. Jeganathan, A. Ghrayeb, L. Szczecinski, and A. Ceron, "Space shift keying modulation for MIMO channels," *IEEE Trans. Wireless Commun.*, vol. 8, no. 7, pp. 3692–3703, Jul. 2009.

[10] A. Ghosh, R. Ratasuk, B. Mondal, N. Mangalvedhe, and T. Thomas, "LTE-Advanced: Next-generation wireless broadband technology," *IEEE Wireless Commun.*, vol. 17, no. 3, pp. 10–22, Jun. 2010.

[11] M. Patzold, *Mobile Fading Channels*. New York, NY: Wiley, 2003.

[12] R. Steele and L. Hanzo, *Mobile Radio Communications*, 2nd ed. New York, NY: Wiley, 1999.

[13] L. Hanzo, O. Alamri, M. El-Hajjar, and N. Wu, *Near-Capacity Multifunctional MIMO Systems (Sphere-Packing, Iterative Detection and Cooperation)*. New York: Wiley, May 2009.

[14] H. G. Myung, J. Lim, and D. J. Goodman, "Single-carrier FDMA for uplink wireless transmission," *IEEE Veh. Technol. Mag.*, vol. 1, no. 3, pp. 30–38, Sep. 2006.

[15] L. L. Yang, *Multicarrier Communications*. Chichester, U.K.: Wiley, Jan. 2009.

[16] A. Wilzeck, Q. Cai, M. Schiewer, and T. Kaiser, "Effect of multiple-carrier frequency offsets in MIMO SC-FDMA systems," in *Proc. Int. ITG/IEEE Workshop Smart Antennas*, Vienna, Austria, Feb. 2007.

[17] L. Hanzo, M. Munster, B. J. Choi, and T. Keller, *OFDM and MC-CDMA for Broadcasting Multiuser Communications, WLANs and Broadcasting*. New York: Wiley, Jul. 2003.

[18] J. R. Barry, E. A. Lee, and D. G. Messerschmitt, *Digital Communication*, 3rd ed. Berlin, Germany: Springer-Verlag, 2003.

[19] S. Alamouti, "A simple transmit diversity technique for wireless communications," *IEEE J. Sel. Areas Commun.*, vol. 16, no. 8, pp. 1451–1458, Oct. 1998.

[20] M. Tuchler, "Design of serially concatenated systems depending on the block length," *IEEE Trans. Commun.*, vol. 52, no. 2, pp. 209–218, Feb. 2004.

[21] J. Hagenauer, "The EXIT chart—Introduction to extrinsic information transfer in iterative processing," in *Proc. Eur. Signal Process. Conf.*, Vienna, Austria, Sep. 2004, pp. 1541–1548.

[22] S. Ten Brink, "Convergence behavior of iteratively decoded parallel concatenated codes," *IEEE Trans. Commun.*, vol. 49, no. 10, pp. 1727–1737, Oct. 2001.

[23] F. Babich, A. Crismani, M. Driusso, and L. Hanzo, "Design criteria and genetic algorithm aided optimization of three-stage concatenated space–time shift keying systems," *IEEE Signal Process. Lett.*, vol. 19, no. 8, pp. 543–546, Aug. 2012.

[24] M. Jiang and L. Hanzo, "Unitary linear dispersion code design and optimization for MIMO communication systems," *IEEE Signal Process. Lett.*, vol. 17, no. 5, pp. 497–500, May 2010.

[25] R. Rajashekar, K. Hari, and L. Hanzo, "Field-extension-code-based dispersion matrices for coherently detected space–time shift keying," in *Proc. IEEE GLOBECOM*, Dec. 2011, pp. 1–5.